A 2D-NUMERICAL STUDY ON SLOT JET APPLIED TO A WIND TURBINE AS A CIRCULATION CONTROL TECHNIQUE

I. Petracci (1,*), L. Manni (2), M. Angelino (3) , S. Corasaniti (1) and F. Gori (1)
(1) University of Rome "Tor Vergata", Via del Politecnico 1, 00133 Rome, Italy
(2) Cecom srl, Via Tiburtina, km 18,700, 00012 Guidonia Montecelio, Rome, Italy
(3) Loughborough University, Aeronautical and Automotive Engineering, Stewart Miller Building, Loughborough LE11 3TU, UK
*Corresponding author: ivano.petracci@uniroma2.it

Keywords: Wind Turbine; S809 Airfoil; Circulation Control; Coanda Slot Jet; 2D k-ω simulation; Power Enhancement;

ABSTRACT

A study on the feasibility of the Circulation Control (CC) technique for wind turbines is proposed. The CC was born in aeronautic field to improve the lift force on the wings, allowing the short take-off and landing of aircraft. It consists in blowing air at a relatively high speed over a rounded trailing edge. The thin jet of air remains attached to the convex curved surface, imposing a certain curvature to the outer streamlines, and, hence, increasing the lift force of the airfoil. Aim of this study is to numerically investigate the advantages on a wind turbine, based on the S809 airfoil, taking into account the energy-related considerations, as the cost of the jet production. The paper, after a thorough evaluation of the increase of the generated power, finds that this technique could be promising in the energy-harvesting aim.

NOMENCLATURE

A	Area [m^2]
C	Chord length [m]
C_D	Drag coefficient
C_L	Lift coefficient
C_{Th}	Thrust coefficient
C_{Tq}	Torque coefficient
Cμ	Jet momentum coefficient
p	Instantaneous static pressure [Pa]
P	Reynolds-averaged static pressure [Pa]
P	Mechanical power [W]
Re	Reynolds number based on the chord length
S_{ij}	Mean rate of strain tensor [1/s]
u_i	component of instantaneous velocity [m/s]
U_i	Reynolds-averaged velocity,component [m/s]
V	Velocity [m/s]

Greek

α	Angle of attack [°]
δ_{ij}	Kroenecker delta
η	Blowing efficiency
ϑ	Sum of twist and pitch angles [°]
k	Turbulent kinetic energy [m^2/s^2]
ν	Kinematic viscosity [m^2/s]
ν_T	Turbulent (or eddy) viscosity [m^2/s]
ρ	Density [kg/m^3]
ω	Specific dissipation rate of turbulent kinetic energy, Rotor angular velocity, [1/s]

INTRODUCTION

Wind represents one of the most promising renewable energy. As every renewable energy source, it is strongly affected by the very low density (i.e., it is required a huge turbine to produce few megawatts) and the discontinuous nature of the wind. To improve the energy conversion efficiency, despite the well-known Betz limit [1], industry and researchers focused their attention on several lift-increasing solutions, form the simplest passive one, such as the Gurney flap, to the active pitch control and the more complicated jet-blowing or Coanda jet.

A submerged jet consists in an unconfined fluid flow issuing from a nozzle into a stagnant region where the same fluid is present. It is a well-known fact in scientific literature that it is able to attract the surrounding stagnant fluid. Tangentially injecting a jet sheet over a rounded trailing edge can cause the boundary layer to adhere further along the curved surface of the airfoil due to the Coanda effect. The rear stagnation point moves toward the pressure side, also, the outer flow is turned substantially, increasing the circulation and thus leading to a higher lift. This phenomenon is explained by the

Kutta-Žukovskij theorem [2], which relates the lift, generated by an airfoil to the freestream velocity, the density of the fluid, and the circulation of the velocity.

The Coanda jet technology is born in aeronautics, and was initially proposed for helicopter rotors [3-4]. Englar and Huson [5] reduced the complexity of the circulation control wings, by evaluating several geometric parameters of the trailing edge, but maintaining the high lift generated and reducing weight and size.

As far as the drag force is concerned, this technique produces a drag penalty, especially on the first design of the circulation-controlled wings, which presents a large trailing edge radius. An effective way to limit this drag is to make flatter the lower surface of the trailing edge, while keeping the upper surface highly curved [6].

In the wind turbines, the torque production is strictly related to the lift of the airfoil, represented by a generic radial section of the blades. The power generation can be obtained as result of the induced thrust forces generated by a forward rotation of the lift vector. Hence, the increase of the lift force corresponds to an increase of the thrust and of the torque. Since the production of the jet requires a power consumption, a net positive increase of the power, generated for Circulation Control, needs to be attractive. It should be noted that the increased lift is not due to the thrust of the jet, because the jet represents a very little mass ejection. The lift enhancement is due to the deflection imposed to the further flow field, that would be otherwise irrotational.

Numerical Investigation of Coanda Jet: The Coanda jet on a circulation controlled airfoil has been numerically investigated, even though there is a paucity of experimental data. The work of Hand et al. [7] represents a milestone for both numerical and experimental studies. They investigated the full-sized NREL Phase VI wind turbine in a very large wind tunnel, producing an unique data set which has been widely employed for comparisons and validation of the turbulence modeling approaches in last decade. This NREL Phase VI wind turbine,designed for experimental purposes, has two twisted and tapered blades, based on the S809 airfoil. The S809 airfoil (as the S-series) is specifically designed for wind turbine applications, and has been proposed and characterized by Somers [8]. The shape of this airfoil is aimed to produce a drag curve, which is almost constant for a wide range of variation of the lift coefficient. The airfoil shape limits the sensitivity to to the transition location, which is a key aspect at relatively low Reynolds numbers.

Taking into account the unique data set of the NREL UAE Phase-VI, as baseline configuration for comparisons, the authors of [9] numerically investigated the Coanda jet effectiveness. In a 3D-study, they observed an increased amount of net power generation for moderate jet momentum coefficients, with the slot jet at the end of the trailing edge. Maldonado et al. [10] tested the synthetic jet actuators to enhance the performance of wind turbine blades by mitigating the flow separation.

Aim of the work: The aim is a preliminary evaluation of Coanda jet as an active technique of circulation control, using 2D simulations that require limited time and resources for calculation. The jets are applied to the upper surface of S809 wing profile, from the leading edge, x/C=0.0, to the trailing edge, x/C=0.95. Two different slot thicknesses and two jet momentum coefficients are tested.

NUMERICAL APPROACH

Governing equations: The governing equations of the flow are the mathematical expression of the conservation laws of mass and momentum. For an incompressible Newtonian fluid, then, these two principles are described by the continuity and momentum equations, also known as Navier-Stokes equations. Whether the flow is turbulent or not, these equations can be written, using the Einstein summation convention, as

$$\frac{\partial u_i}{\partial x_i}$$

$$\frac{\partial u_i}{\partial t} + u_j \frac{\partial u_i}{\partial x_j} = -\frac{1}{\rho}\frac{\partial p}{\partial x_i} + \nu \frac{\partial^2 u_i}{\partial x_i \partial x_j}$$

After performing the Reynolds average (or ensemble average) on both terms of the equations, we obtain the Reynolds-Average Navier-Stokes equations (RANS):

$$\frac{\partial U_i}{\partial x_i}$$

$$\frac{\partial U_i}{\partial t} + U_j \frac{\partial U_i}{\partial x_j} = -\frac{1}{\rho}\frac{\partial P}{\partial x_i} + \frac{\partial}{\partial x_j}\left(\nu \frac{\partial U_i}{\partial x_j} - \overline{u_i' u_j'}\right)$$

where the extra terms $\overline{u_i'u_j'}$ are the Reynolds stress tensors, which cannot be calculated directly from the mean motion of the fluid and needs to be modeled. In present work, the linear constitutive relationship is adopted, with the mean flow rate of strain tensor, as suggested by Boussinesq's hypothesis:

$$-\overline{u_i'u_j'} = 2\nu_T S_{ij} - \frac{2}{3}k\delta_{ij}$$

The turbulent viscosity is modeled with the SST version of k – ω turbulence model, proposed by Menter [11]. The two transport equations of this model are

$$\frac{\partial k}{\partial t} + U_j \frac{\partial k}{\partial x_j} = P_k - \beta^* k\omega + \frac{\partial}{\partial x_j}\left[\left(\nu + \sigma_k \nu_T\right)\frac{\partial k}{\partial x_j}\right];$$

$$\frac{\partial \omega}{\partial t} + U_j \frac{\partial \omega}{\partial x_j} = \alpha S^2 - \beta\omega^2 + \frac{\partial}{\partial x_j}\left[\left(\nu + \sigma_\omega \nu_T\right)\frac{\partial \omega}{\partial x_j}\right] + 2\left(1 - F_1\right)\sigma_{\omega,2}\frac{1}{\omega}\frac{\partial k}{\partial x_i}\frac{\partial \omega}{\partial x_i}$$

which allow to compute for turbulent viscosity by using the following relation

$$\nu_T = \frac{a_1 k}{\max\left[\alpha_1 \omega, SF_2\right]}$$

where S is the strain rate and F_1 and F_2 are blending functions. Further details for what concerns constants and other terms definitions can be found in [11].

The flow is modeled as incompressible and steady, therefore a pressure-velocity coupling strategy is required for solving the equations. As far as the solver is concerned, the SIMPLE algorithm [12] is used. As far as the spatial discretization is concerned, the convective terms are treated with the linearUpwind scheme, which allows to achieve a second order accuracy. The OpenFOAM open-source code is used to solve all the discretized equations.

Computational domain and boundary conditions: The computational domain is designed similarly to the test section of the wind tunnel present in the Laboratory of Thermal Sciences and Energy Engineering of the University of Rome "Tor Vergata", in order to allow future comparisons with experiments.

Figure 1 shows the computational domain, which is 2.5 chords in highness and 13 in length. The distance of 6 chords upstream the leading edge is necessary in order to achieve the independence of the turbulent variables with respect to the inlet boundary conditions. Similarly, the outlet is 6 chords downstream to prevent contamination of the non-physical disturbances from the computational boundary to the solution. As far as the top and bottom walls of the wind tunnel are concerned, a slip boundary condition is applied, as the boundary layer, in the actual wind tunnel, is fully developed and a fine mesh is not required by the solver.

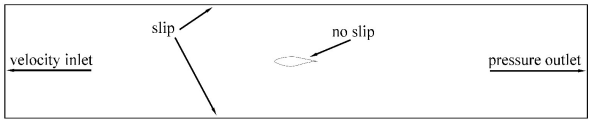

Figure 1 – Scheme of the computational domain

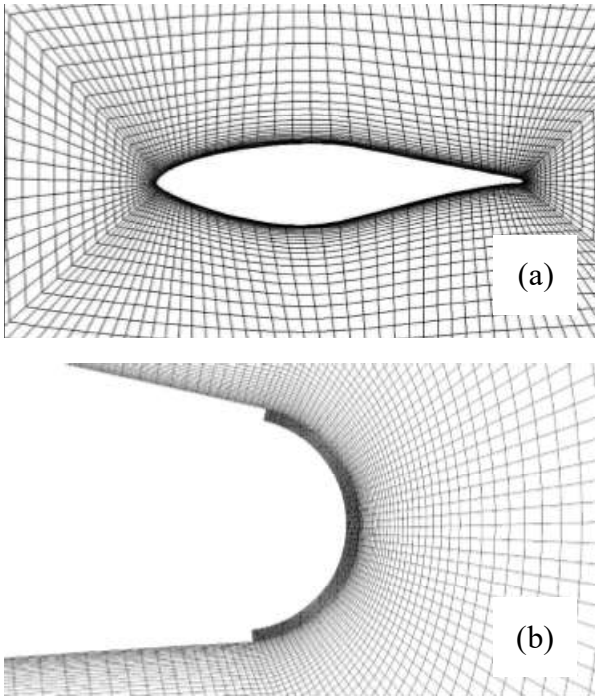

Figure 2 – Details of the mesh of the airfoil S809. (a) O-grid mesh close to the profile (a line every 4 is represented); (b) slot exit at $x/C = 0.95$.

The mesh is made of three blocks. The first one is from the inlet and to 1 chord upstream with respect to the leading edge. The second one extends from this point up to 1 chord downstream the leading edge. The third one, identical to the first one, is placed from the end of the second block to the outlet. The second block is O-grid splitted to host the airfoil and to follow the curvature. The airfoil is

truncated at 95% of the chord and a rounded trailing edge is provided. A close-up of the mesh, around the airfoil, is shown in Figure 2a.

Close to the wall profile, the height of the first cell is fixed to achieve y+≈1, to correctly solve the boundary layer up to the viscous sub-layer. The slot is modelled by introducing another block underneath the edge corresponding to the airfoil surface. In the chord-wise direction the mesh is refined in close proximity to the slot exit, whereas, in the surface-normal direction, the cells have the same height of the slot exit, then a growth ratio of 1.1 is adopted. Some details of the mesh, close to the slot exit at x/c=0.95, is provided in Fig. 2b.

Dynamic actions and numerical validation on the base profile: The results proposed in this section are not supposed to highlight the physics aspects involved in the Coanda Jet, neither this 2D study aims to explain deeply the origin of the induced benefits.

The present numerical investigation aims to show how much the performance increase is linked to the geometrical and kinematic features. The lift curves are firstly analyzed, because the lift force is directly involved in the torque production of the turbine, as shown in Fig. 3.

Figure 3 shows the dependence of the torque force T_q from the lift L and the drag D forces of the profile. The first one gives a positive contribution, whereas the second one has a component directed opposite to the rotation, with a negative contribution.

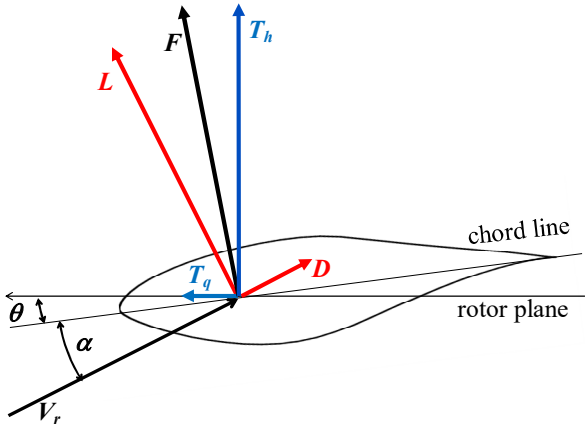

Figure 3 – Decomposition of aerodynamic forces

The angle of attack α of Fig. 3 is the angle formed between the opposite of the wind speed vector (i.e., flight velocity vector) and the chord of the profile. According to this definition, lift and drag forces are expressed as

$$L = F\cos\alpha$$

$$D = F\sin\alpha$$

Usually, aerodynamics forces are normalized with the dimensios of the flow characteristics, and the information about the shape of the profile, useful for designers. The non-dimensional lift and drag coefficients are defined as

$$C_L = \frac{L}{\frac{1}{2}\rho V_r^2 C\Delta z}$$

$$C_D = \frac{D}{\frac{1}{2}\rho V_r^2 C\Delta z}$$

where C is the chord length and Δz the spanwise extension of the wing. The denominator of both equations represents the force that would act on the wing if the dynamic pressure is applied to a rectangular surface with C and Δz as dimensions.

The ratio between lift and drag coefficients is defined as profile efficiency.

The behavior of the lift and drag coefficients with respect to the angle of attack is a fundamental aspect of an airfoil, but, in order to understand the pattern, one can analyze the pressure coefficient, defined as

$$C_P = \frac{p_x - p_\infty}{\frac{1}{2}\rho V_r^2}$$

where p_∞ represents the freestream pressure. Maximum pressure coefficient is always equal to 1, on the profile, and corresponds to stagnation pressure.

For future comparisons, the relative velocity is chosen according to the experimental wind tunnel limit, that is 20 ms^{-1}. As consequence, the simulated Reynolds number is equal to

$$\mathrm{Re} = \frac{V_r^2 C}{\nu} = 2.5\cdot 10^5$$

The coefficient of the jet momentum,a non-dimensional parameter which identifies the momentum of the Coanda jet, is defined as

$$C_\mu = \frac{\dot{m} V_{jet}}{\frac{1}{2}\rho V_{ref}^2 A_{ref}}$$

where $\dot{m} = \rho_{jet} A_{jet} V_{jet}$ is the mass flow rate of the jet, V_{ref} is the rotor tip speed and A_{ref} is the platform area of the rotor blade, given by the chord length

integral along the blade axis. In the present 2D simulations the rotor tip speed coincides with the relative velocity.

As far as numerical studies are concerned, most relevant 2D simulations have been performed by Djojodihardjo et al. [13] and by Kang and Park [14], both focused on the S809 airfoil, by testing several positions of the jet and varying the jet momentum coefficient.

The present work, taking advantage of the little time required by the 2D simulations, tests several configurations in order to find the best solution to apply to the full size turbine. Table 1 provides a summary of the tested cases, with a comparison with the literature [13-14].

The jet height is equal to 10^{-4} m and $5 \cdot 10^{-5}$ m, which correspond to 0.05% and 0.025% of the chord length. The velocity on the slot exit is changed to vary the jet momentum coefficient, $C\mu$. The limit of the tested $C\mu$ configurations is given by the Mach number on the slot exit, which must be smaller than 0.3 to use an incompressible solver. The jet position varies from x/C = 0.00, the jet is placed at leading edge, till x/C = 0.95, which corresponds to the jet placed exactly between the end of the suction side and the rounded trailing edge.

The numerical results, in the case with $C\mu$=0 (i.e. without jet), are validated with the comparison with the experimental ones of Taylor [15], where an S809 wing profile is tested at Reynolds number equal to $2.2 \cdot 10^5$, which is very close to that of this work. The comparison is reported in Fig. 4. The graph shows a good match for the lift coefficient up to the stall angle. The maximum profile efficiency is obtained at the same angle of attack, i.e. 7°.

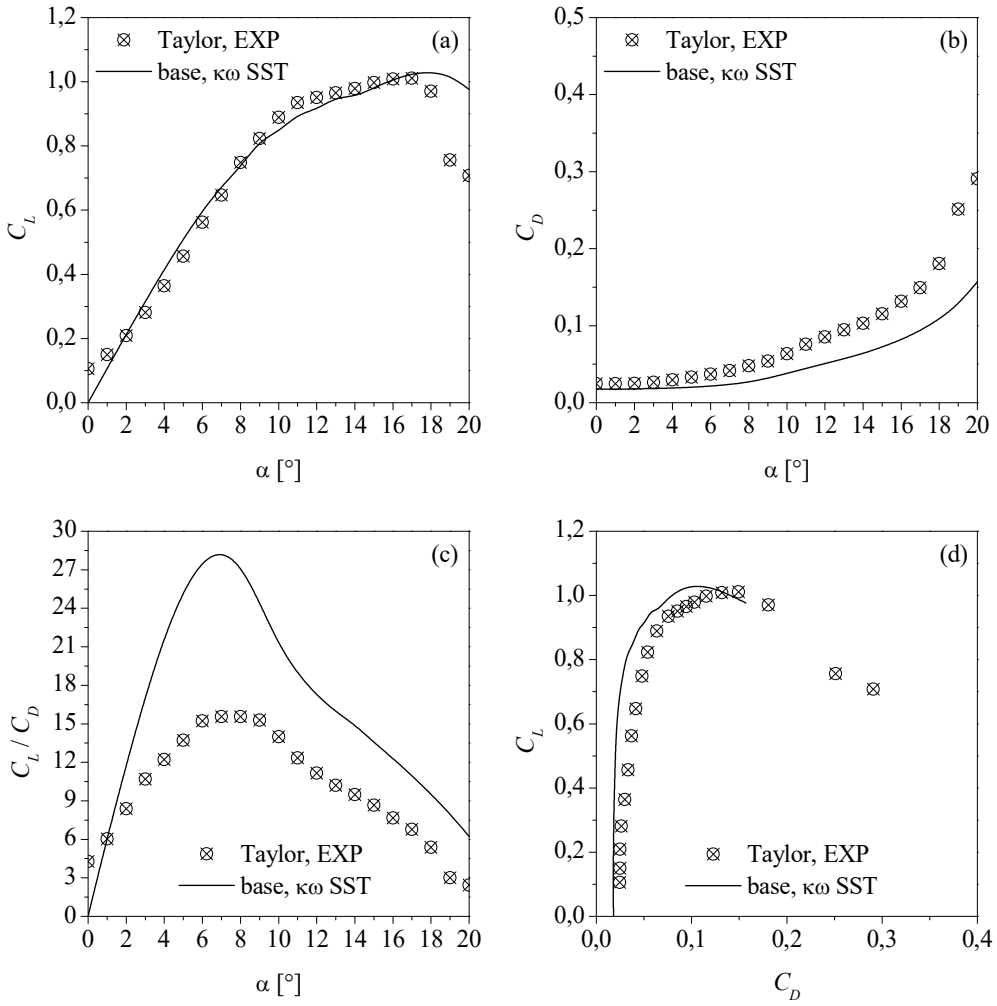

Figure 4 - Comparison between the numerical CFD results of this work and the experiments of [15] for the base profile (without jet)

Table 1
Summary and comparison with most relevant 2D studies of circulation controlled S809 airfoil.

Author	Re	Chord, *C* [m]	y+	Turbulence Model	Jet position, *x/C*	t_{jet} [mm]	Jet BC	C_μ
Kang [14]	$2\cdot10^6$	0,6	1	Spalart-Allmaras	0,025-0,6-0,8-0,9	3	Pressure inlet	//
Djojodihardjo [13]	$4\cdot10^5 – 10^6$	1	11,06	κ-ε standard	0,9-0,95	1 – 3	Velocity inlet	0,05
This Work	$2.5\cdot10^5$	0,2	≈1	κ-ω SST	0,0-0,2-0,4-0,6-0,95	0.05 – 0.1	Velocity inlet	0,01 – 0,015

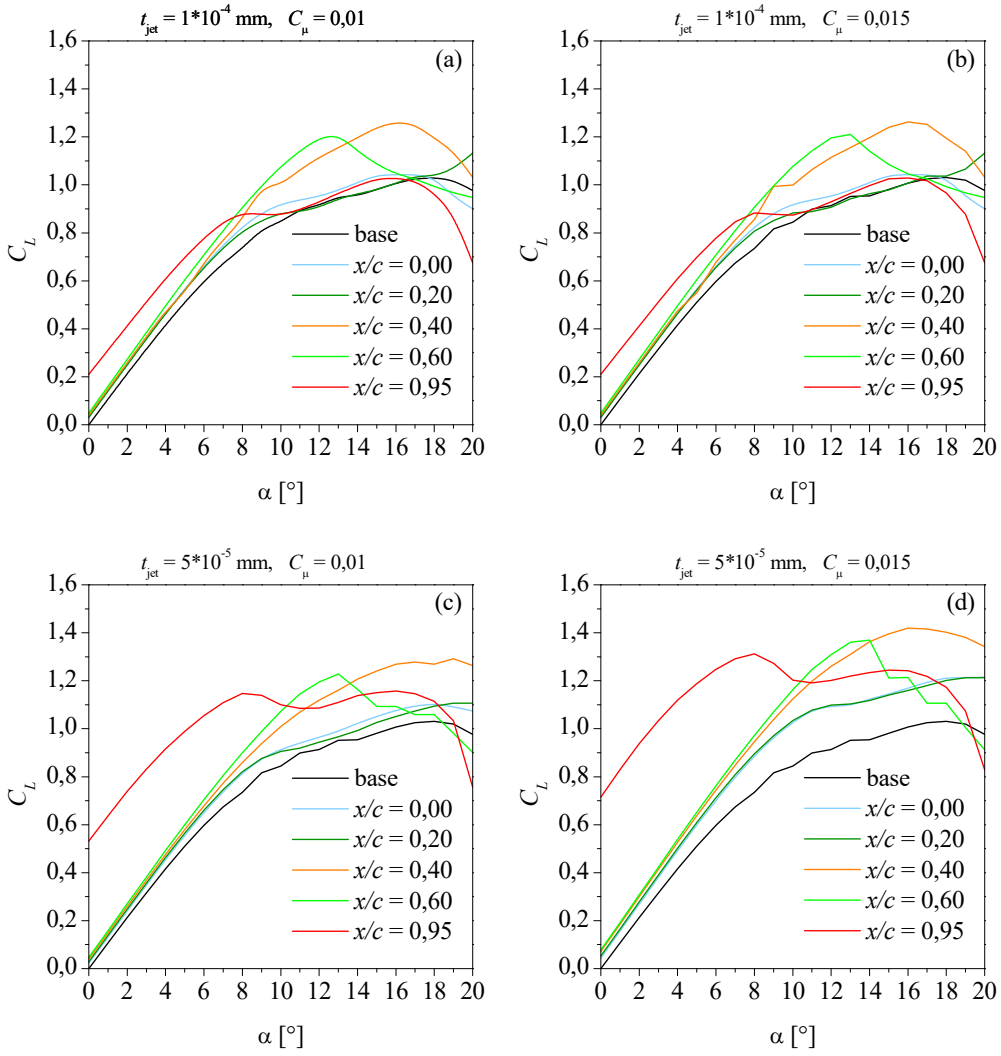

Figure 5 – Lift curves for all cases.

RESULTS AND DISCUSSION

Lift Curves: The lift curves are shown in Fig. 5 enlightening two fundamental aspects of the behavior of the Coanda Jet. First, the magnitude of the lift improvement depends more on the parameter *Cμ* rather than the slot height, even though they are linked by the *Cμ* definition. The second aspect is the effect of the jet position, which does not affect the magnitude of the lift enhancement (except for *x/C*=0.95). If the jet is placed upstream the angle of attack with the maximum lift is shifted.

This observation offers several perspectives for a future implementation. The realization of the blowing system is a significant complication introduced on a relatively simple machine, as the wind turbine. The presence of a secondary slot, on

the suction side, could modulate the blowing position, following the wind conditions. This possibility could improve greatly the performance of the double-blowing system, compared to the single-blowing one. Furthermore, the complication for the realization of the secondary slot can be reduced and carried out almost without additional costs. Moreover, the usefulness of a suction side slot, near the leading edge, is twofold. Indeed, it can be employed as a de-icing system. Since the depression zones are more susceptible to the ice formation, the suction side slot, or, eventually, a leading edge slot could blow heated air, for example taken from the nacelle, where the friction in the gerabox would be enough to enhance its temperature by few degrees.

When the slot is placed on the trailing edge (i.e. x/C=0.95), a significant lift enhancement is observed from 0° to 15° of angle of attack, which decreases almost linearly. The thinner slot produces the most encouraging results, with a lift coefficient which is more than twice the base one. The improvement of the performance at low angle of attacks is preferred because corresponds to the low wind speeds, and Phase-VI is a stall-regulated wind turbine which cut the power at high wind speeds by stalling from the center to the tip. Within the x/C=0.95 cases, the difference in terms of lift production is quite small between the two values of $C\mu$ evaluated. The slot height, instead, seems to affect the performances more significantly: the thinner the slot, the higher the lift. However, a thinner slot does not directly imply a lower power required by the blowing system, because the $C\mu$ definition contains the slot height and the power depends on the cube of the jet speed. Indeed, comparing the two slots, the lower power consumption is given by the thicker slot, since the cube of the velocity ratio is almost 2.8, whereas the slot height ratio is 0.5.

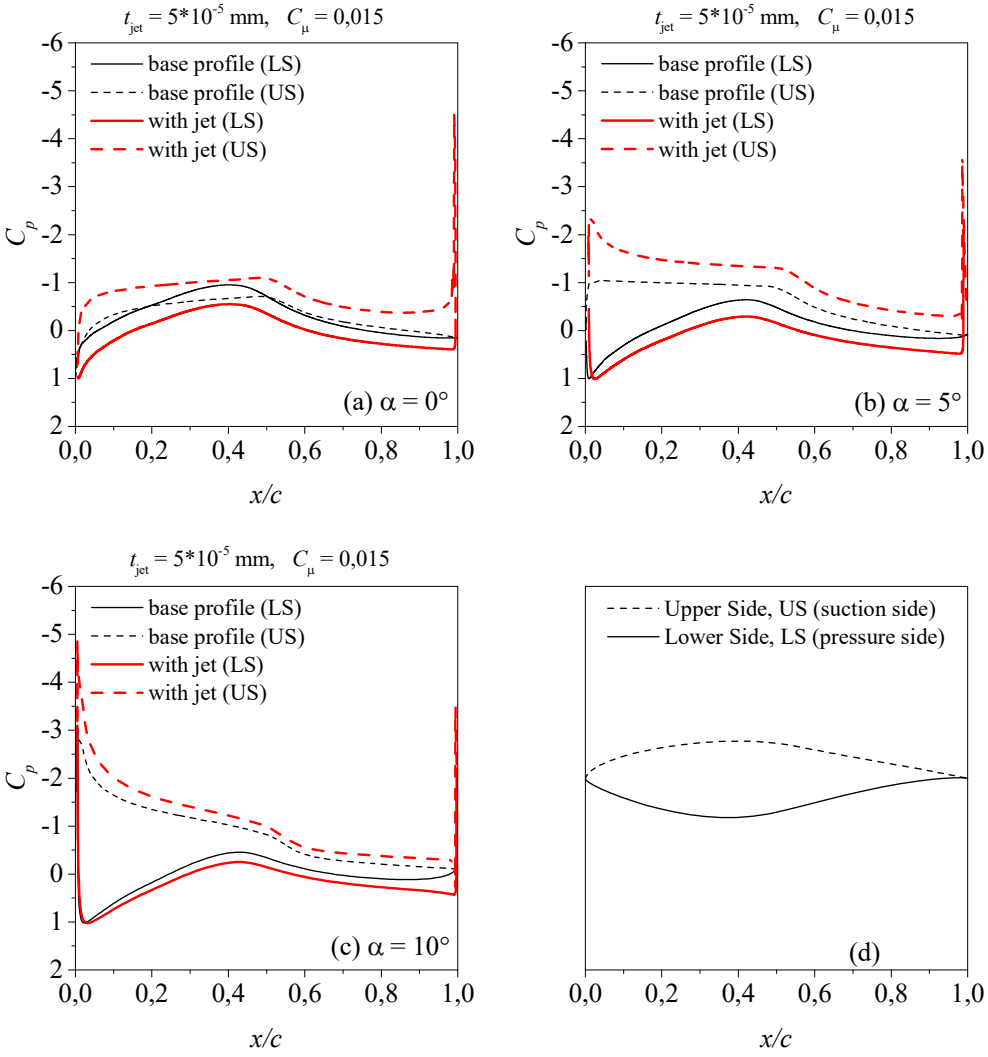

Figure 6 – Pessure profile: baseline vs profile with jet at x/C=0.95

Pressure coefficient: The pressure coefficient is shown in Fig. 6 for some angles of attack. The lift coefficient is proportional to the area inside the curves, and these plots highlight the reason for the jet effectiveness at lower angles of attack. A suction peak is present at the leading edge up to 10°, which appears already at 5° when the jet is active, whereas the pressure coefficient of the airfoil, without the jet, somewhat resembles the 0° case. This leads to the speculation that the jet acts increasing the effective angle of attack, or by shifting the lift curve to the left. Once the angle of attack is high enough, the effectiveness of the jet is reduced. For angles of attack higher than 15°, the conclusions could be different, as massive separation occurs and 2D simulations could not be reliable.

Estimation of power generated: The Blade Element Momentum theory (BEM) has been used in this section to predict the increase in the power generation by means of the 2D simulations. BEM theory is obtained from the Blade Element Theory (BET) by the introduction of the momentum theory and considering the rotation. In the BEM theory, we consider the rotor as the summation of a series of annular rings, one independent from the other. This theory does not account for the tip losses, wake expansion and yaw, and is based on the steady flow. Under these assumptions, and by considering the aerodynamic forces acting on the sections of the blade, the torque can be computed as the integral of the resulting moments of lift and drag projections on the rotation plane, with respect to the rotation axis. Once the torque is known, the computation of the power is straightforward, as the turbine is supposed to work at constant angular rotation velocity.

Considering the symbols used in Fig. 3, the torque and thrust coefficients can be defined as

$$C_{Th} = C_L \cos(\alpha + \vartheta) + C_D \sin(\alpha + \vartheta)$$

$$C_{Tq} = C_L \sin(\alpha + \vartheta) - C_D \cos(\alpha + \vartheta)$$

where α is an aerodynamic angle which depends on the wind conditions, whereas ϑ is the effective local constructive angle, given by the sum of the local twist angle and the blade pitch angle.

The C_{Th} coefficient represents the axial non-dimensional thrust which is a mechanical load for the wind turbine structure, whereas the C_{Tq} is the non-dimensional net torque generated by the lift and drag projections on the plane of rotation.

In order to obtain the actual tangential force produced by the infinitesimal element of the blade, the following expression can be used:

$$dF_{Thrust} = \frac{1}{2}\rho C \cdot C_{Tq} V_{ref}^2 dr$$

where C and dr are the chord length and the spanwise elementary extension, respectively, and the freestream velocity experienced by the blade section coincides with the inlet velocity for 2D simulations.

As far as the torque is concerned, every section gives an elementary contribution, given by

$$dT = \frac{1}{2}\rho C \cdot C_{Tq} V_{ref}^2 r dr$$

where r denotes the distance from the center of the rotor. In order to compute the power production, the expression of total torque is necessary and it can be obtained integrating over the blade as

$$P = \omega \int_{r0}^{R} \frac{1}{2}\rho C \cdot C_{Tq} V_{ref}^2 r dr$$

Assuming a small wind turbine, with geometrical details reported in Tab. 2, the integral is solved by the use of a polynomial function. These dimensions are calculated on the basis of the study of Giguere and Selig [16], by scaling the problem in order to have a chord small enough to be experimentally investigated.

A series of 2D simulations are carried out, with a wind speed of 7 m/s.

Table 2
Examples of geometry of a small wind turbine

r [m]	r/R	C [m]	α [°]	V_r [m/s]
0.61	0.30	0.28	11.55	8.86
0.94	0.47	0.25	10.84	10.15
1.26	0.63	0.22	10.94	12.15
1.50	0.75	0.19	11.13	13.70
1.92	0.96	0.15	11.23	16.66
2.00	1.00	0.14	11.20	17.20

In order to evaluate the power consumption, required by the jet production, a blowing efficiency is considered. Consequently, the power can be expressed as

$$P_{jet} = \left[\frac{1}{2}\dot{m}_{jet} V_{jet}^2\right] \Big/ \left[\eta_{blowing}\right] = \left[\frac{1}{2}\rho_{jet} A_{jet} V_{jet}^3\right] \Big/ \left[\eta_{blowing}\right]$$

where η_{blowing} is the blowing efficiency, assumed equal to 0.85. The jet is placed at x/C=0.95.

The results, for the estimated increment of power, are provided in Tab. 3. The values are compared with the baseline case (without jet), for which the supplied power is P_{base}=0.117 kW, while the power increment is defined as

$$\Delta P = \left[\left(P - P_{jet}\right) - P_{base}\right] \Big/ \left[P_{base}\right]$$

Table 3
Power generation estimated by 2D simulations

x/C	0.95	0.40	0.95	0.40
t_{jet} [mm]	0.05	0.05	0.1	0.1
$C\mu$	0.015	0.015	0.01	0.01
V_{jet} [m/s]	103.6	109.5	59.80	63.25
P_{jet} [kW]	0.077	0.091	0.029	0.035
P [kW]	0.163	0.173	0.166	0.152
ΔP [%]	-26.5	-29.9	16.6	0.5

As can be seen, the power required by the jet is related to the cube of its velocity, thus the weight of this parameter strongly affects the performance. Indeed, an encouraging result is the 16.6% of increment in power, corresponding to the lowest jet velocity tested.

CONCLUSIONS

In the present study, the feasibility of the Circulation Control technique for wind turbines is investigated with 2D numerical simulations. Coanda jets are applied to the upper surface of a S809 wing profile, from the leading edge, x/C=0.0, to the trailing edge, x/C=0.95. Two different slot thicknesses and two jet momentum coefficients are tested.

Results are encouraging, at least for a further numerical investigation of this technique. At low wind speed (i.e. 7 m/s), the increase of power is 16.6% compared to the base power production, also considering the energy consumption of the jet, which has been considered by introducing a blowing efficiency of 0.85. The presence of the jet is shown to be ineffective at higher wind speeds, suggesting that the Coanda jet works only when flow is fully attached, or at least, some slight separation near the stall point occurs.

The blowing jet, installed close to the leading edge, delays the stall angle, and could be useful also for other purposes, such as the de-icing system.

REFERENCES

1. A. Betz and D. G Randall, 1966, Introduction to the theory of flow machines.
2. J. D. Anderson, 2012, Introduction to flight. McGraw Hill, New York, 7th ed.
3. R. L. L. Englar,1975, Circulation Control for High Lift and Drag Generation on STOL Aircraft. Journal of Aircraft, 12(5):457–463.
4. J. B. Wilkerson, K. R. Reader, and D. W. Linck. The Application of Circulation Control Aerodynamics to a Helicopter Rotor Model, J. of the American Helicopter Society, 19(2):2, 1974.
5. R. J. Englar and G. Huson,1984, Development of advanced circulation control wing high-lift airfoils. Journal of Aircraft, 21(7):476–483.
6. R. Englar, 2000, Circulation control pneumatic aerodynamics: blown force and moment augmentation and modification - Past, present and future. AIAA Paper 2000-2541.
7. Hand, M. M., Simms, D. A., Fingersh, L. J., Jager, D. W., Cotrell, J. R., Schreck, S., and Larwood, S. M., 2001, "Unsteady Aerodynamics Experiment Phase VI: Wind Tunnel Test Configurations and Available Data Campaigns,"NREL/TP-500–29955, Golden, CO
8. D. Somers, M.,1997, Design and Experimental Results for the S809 Airfoil. NREL/SR-440-6918.
9. C. Tongchitpakdee, S. Benjanirat, and L. Sankar, 2006, Numerical Studies of the Effects of Active and Passive Circulation Enhancement Concepts on Wind Turbine Performance. J. Sol. Energy Eng 128(4), 432-444
10. V. Maldonado, J. Farnsworth, W. Gressick, and M. Amitay, 2008, Active Enhancement of Wind Turbine Blades Performance. AIAA 2008-1311
11. F. R. Menter, 1994, Two-equation eddy-viscosity turbulence models for engineering applications. AIAA Journal, 32(8):1598–1605.
12. S. V. Patankar, 1980, Numerical heat transfer and fluid flow. Series in computational methods in mechanics and thermal sciences. Hemisphere Publ. Co, New York.
13. H. Djojodihardjo, M. F. Abdul Hamid, A. A. Jaafar, S. Basri, F. I. Romli, F. Mustapha, A. S. Mohd Rafie, and D. L. A. Abdul Majid, 2013, Computational Study on the Aerodynamic Performance of Wind Turbine Airfoil Fitted with Coanda Jet. J. of Renewable Energy, 2013:1–17.
14. T. J. Kang and W. G. Park, 2013, Numerical investigation of active control for an S809 wind turbine airfoil. Int. J. of Precision Engineering and Manufacturing, 14(6):1037–1041
15. K. Taylor, C. M. Leong and M. Amitay, 2014, "Load control on a dynamically pitching nite span wind turbine blade using synthetic jets". Wind Energy, pp. 1-17.
16. P. Giguere and M. S. Selig, 1999, Design of a tapered and twisted blade for the NREL combined experiment rotor. NREL/SR- 500-26173, NREL, Golden, CO